



Cite this: RSC Adv., 2017, 7, 39657

Received 13th May 2017  
 Accepted 5th August 2017

DOI: 10.1039/c7ra05429g  
[rsc.li/rsc-advances](http://rsc.li/rsc-advances)

## Multi-band visible photoresponse study of $\text{Co}^{2+}$ doped $\text{ZnO}$ nanoparticles

Anju Anna Jacob,<sup>a</sup> L. Balakrishnan, <sup>bc</sup> K. Shambavi<sup>d</sup> and Z. C. Alex<sup>e</sup>

In this article, near UV (NUV) and near UV-visible photodetectors (PDs) were fabricated using pure ( $\text{ZnO}$ ) and  $\text{Co}$  doped  $\text{ZnO}$  ( $\text{Zn}_{1-x}\text{Co}_x\text{O}$ ) nanoparticles synthesised by co-precipitation method. The structural, morphological, compositional and chemical state analysis of the nanoparticles were done using X-ray diffractometry, transmission electron microscopy, energy dispersive spectrometry and X-ray photoelectron spectrometry respectively. The optical spectra which were recorded using a UV-Vis spectrometer exhibited the presence of absorption peaks in the visible region for  $\text{Co}$  doped  $\text{ZnO}$  due to d-d transitions. Enhanced photoresponse in the NUV region was found in lower doping concentrations and all the  $\text{Co}$  doped  $\text{ZnO}$  photodetectors showed a noticeable response to visible light sources. A maximum responsivity of  $63 \text{ mA W}^{-1}$  and quantum efficiency of  $\sim 20\%$  was achieved in the NUV region for the PD fabricated with 2 at%  $\text{Co}$  doping. The 2 at%  $\text{Co}$  doped  $\text{ZnO}$  based photodetector showed efficiency in the range 11–35% for the wavelengths from 401 to 634 nm.

## 1. Introduction

Semiconductor based photodetectors (PDs) have caught much research attention for the past few decades. In recent years much effort has been devoted to  $\text{ZnO}$  owing to its remarkable and unique opto-electronic properties, non-toxicity, high thermal and chemical stability, ability for use in harsh environments, radiation hardness, eco friendliness, low cost, availability etc.  $\text{ZnO}$  is an intrinsically n-type semiconductor having a hexagonal wurtzite structure with a large direct band gap of  $\sim 3.37 \text{ eV}$ . It exhibits a large excitonic binding energy of  $\sim 60 \text{ meV}$  at room temperature.<sup>1–4</sup> The wide band gap limits its light absorption at the near ultra-violet (NUV) region, hence  $\text{ZnO}$  is most preferred for UV light detection and many works have reported on the fabrication of  $\text{ZnO}$  based UV PDs.<sup>5–8</sup> Through the suitable addition of impurities through doping or alloying, the properties of  $\text{ZnO}$  can be effectively controlled and also the absorbing spectral region can be shifted or extended.<sup>9–11</sup> Many research groups have reported the fabrication of  $\text{ZnO}$  based PDs in the deep UV region by increasing the bandgap with Mg doping.<sup>12–14</sup> Recently, Shewale *et al.* reported the fabrication of Mg doped  $\text{ZnO}$  nanorod array film based PDs

by pulsed laser deposition (PLD) at different growth times and achieved a maximum responsivity of  $22.33 \text{ mA W}^{-1}$ .<sup>15</sup>

Considering the wide range of applications like flame detection, environmental monitoring and image sensing, visible light detection is also much necessary and the works on  $\text{ZnO}$  based visible detectors are very few.<sup>16</sup> With Cd doping, the bandgap of  $\text{ZnO}$  can be red shifted to extend the absorption towards blue region; still further shifting is again limited.<sup>17,18</sup> In our previous work, with Cd alloying the  $\text{ZnO}$  thin film band gap was shifted to  $2.66 \text{ eV}$  and the fabricated PDs exhibited enhanced photoresponse in NUV and blue regime.<sup>19</sup> Studies on the optical properties of  $\text{Co}$  doped  $\text{ZnO}$  reports the presence of absorption peaks in the visible region due to 3d ligand field split states.<sup>20–22</sup> This can be utilized for the fabrication of visible light detectors without losing the other advantages of  $\text{ZnO}$ . Also, doping with transition metals like  $\text{Co}$  hinders the recombination of electron hole pair generated from optical absorption which also improves the optical properties of  $\text{ZnO}$ .<sup>23</sup> The ionic and covalent radius of  $\text{Co}$  ( $0.072 \text{ nm}$  and  $0.116 \text{ nm}$ ) matches with that of  $\text{Zn}$  ( $0.074 \text{ nm}$  and  $0.125 \text{ nm}$ ), so it can be properly alloyed to the lattice without disturbing the crystal structure of  $\text{ZnO}$  and not much changing the lattice strain. Johnson *et al.* studied the temperature dependant visible light photoconductivity of  $\text{ZnO}$  films with varying  $\text{Co}$  doping concentration and obtained maximum light conversion efficiency at lower concentration, which is much smaller than the achievable solubility limit of  $\text{Co}^{2+}$  ions in  $\text{ZnO}$  lattice.<sup>24</sup> So far, no works have been reported on the fabrication of  $\text{Co}$  alloyed  $\text{ZnO}$  visible light detectors. The present work aims at analysing the material properties of pure and  $\text{Co}$  alloyed  $\text{ZnO}$ , and attempts

<sup>a</sup>School of Electronics Engineering, VIT University, Vellore 632 014, India

<sup>b</sup>Department of Physics, Government College of Technology, Coimbatore 641 013, India

<sup>c</sup>Department of Physics, School of Advanced Sciences, VIT University, Vellore 632 014, India. E-mail: [bslv85@gmail.com](mailto:bslv85@gmail.com); Tel: +91-9944881875

<sup>d</sup>Department of Communication, School of Electronics Engineering, VIT University, Vellore 632 014, India

<sup>e</sup>Department of Sensor and Biomedical Technology, School of Electronics Engineering, VIT University, Vellore 632 014, India



for the first time to fabricate PDs for detection in NUV as well as visible regime.

## 2. Materials and methods

ZnO nanoparticles were synthesised by co-precipitation method using zinc acetate di-hydrate ( $\text{Zn}(\text{CH}_3\text{COO})_2 \cdot 2\text{H}_2\text{O}$ ), cobalt chloride ( $\text{CoCl}_2$ ) and sodium hydroxide ( $\text{NaOH}$ ) as precursors. 0.2 M zinc acetate di-hydrate and cobalt chloride corresponding to Co/Zn atomic percentage of 0, 1, 2, 3, and 4 were dissolved in 100 ml deionized (DI) water for the synthesis of  $\text{Zn}_{1-x}\text{Co}_x\text{O}$  for  $x = 1, 2, 3$  and 4 respectively. 0.4 M  $\text{NaOH}$  prepared in 100 ml DI water was added to it drop wise and the resultant solution with precipitate was stirred for 4 h again. The precipitate was washed many times in DI water and ethanol followed by filtering and drying at 150 °C for 1 h. The  $\text{Zn}_{1-x}\text{Co}_x\text{O}$  nanoparticles thus obtained were annealed in muffle furnace at 500 °C for 2 h.

The material properties of synthesised nanoparticles were investigated using X-ray diffractometer (XRD), transmission electron microscope (TEM), energy dispersive spectrometer (EDS), X-ray photoelectron spectrometer (XPS) and UV-Vis spectrometer in Diffuse Reflectance Spectroscopy (DRS) mode. For the fabrication of PDs 10 mm circular pellets of these nanoparticles were made using pelletizer at an applied pressure of 80 kg  $\text{cm}^{-2}$  followed by annealing at 500 °C for 2 h to densify

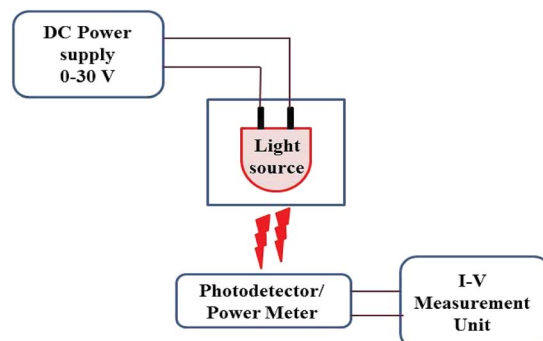


Fig. 2 Schematic of LED power measurement and photodetection studies of PDs.

the pellet, interdigitated electrodes were made over the pellet using silver paste. Photo-response behaviour of PDs towards different wavelength lights were studied using Agilent B2901A Precision *I-V* (current-voltage) measurement unit with UV and visible LEDs as light source. The measuring procedure and details of the source LED parameters were explained in our previous work.<sup>19</sup> The wavelength and power values of LED sources are given in Fig. 1 and Table 1, respectively. The combined schematic for power measurement of LEDs and photoresponse studies of fabricated PDs is shown in Fig. 2.

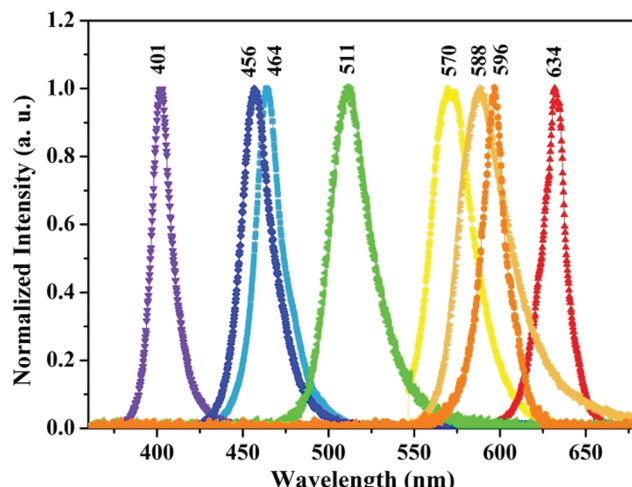


Fig. 1 Emission spectra of LED light sources.

## 3. Results and discussions

### 3.1. Characterization of $\text{Zn}_x\text{Co}_{1-x}\text{O}$ nanoparticles

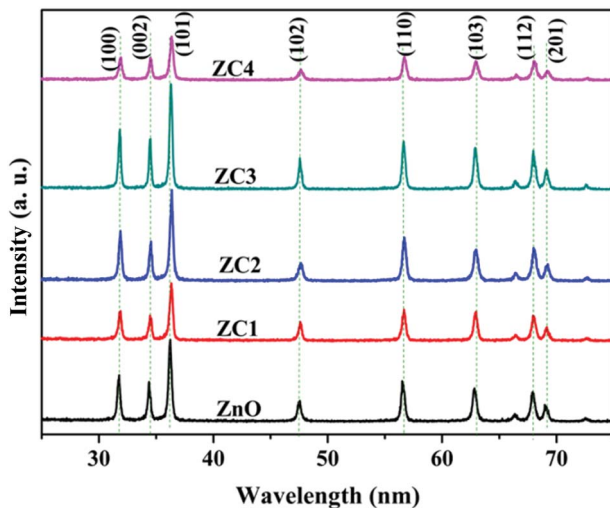
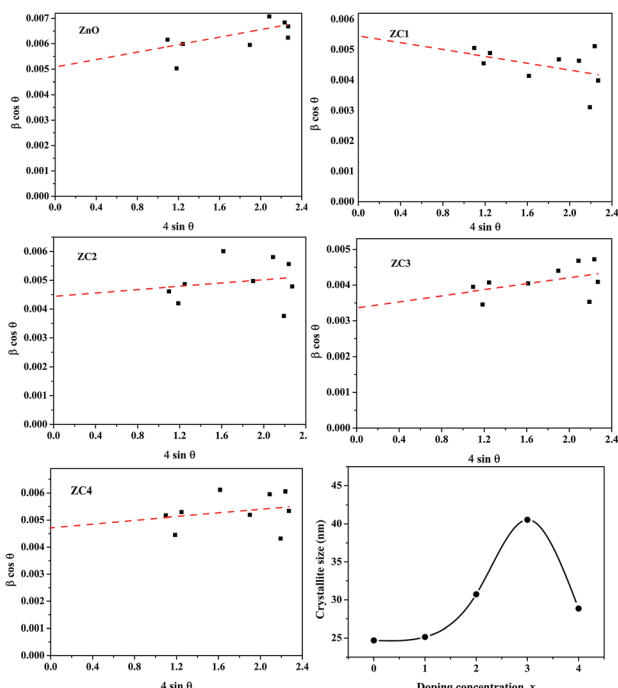
ZnO nanoparticles alloyed with Co ( $\text{Zn}_{1-x}\text{Co}_x\text{O}$ ) at 1, 2, 3 and 4 atomic percentages ( $\text{Zn}_{0.99}\text{Co}_{0.01}\text{O}$ ,  $\text{Zn}_{0.98}\text{Co}_{0.02}\text{O}$ ,  $\text{Zn}_{0.97}\text{Co}_{0.03}\text{O}$  and  $\text{Zn}_{0.96}\text{Co}_{0.04}\text{O}$ ) are represented as ZC1, ZC2, ZC3 and ZC4 respectively.

The XRD pattern shown in Fig. 3 confirms the formation of  $\text{Zn}_{1-x}\text{Co}_x\text{O}$  nanoparticles with hexagonal wurtzite structure. No additional peaks have been observed in Co alloyed nanoparticles indicating the absence of secondary phase formation like CoO or Co-metal/metal clusters. Also, the crystallinity of ZnO has not changed much after Co addition which can be attributed to the substitution of similar ionic radii  $\text{Co}^{2+}$  in  $\text{Zn}^{2+}$  site. The observance of sharp peaks indicates the high crystalline nature of synthesized nanopowders. The average crystallite

Table 1 Output power of LED sources at different forward voltages

Forward voltage, $V$ (volts) and output power, $P$ (mW) for different LED sources															
401 nm		456 nm		465 nm		511 nm		570 nm		588 nm		596 nm		634 nm	
$V$	$P$	$V$	$P$	$V$	$P$	$V$	$P$	$V$	$P$	$V$	$P$	$V$	$P$	$V$	$P$
3.2	3.46	2.8	1.038	2.6	0.12	3.2	1.33	2.2	1.88	2	0.395	2.2	0.777	1.8	0.2
3.4	11.02	3	6.18	2.8	1.2	3.4	2.33	2.4	6.155	2.2	1.086	2.3	1.271	1.9	0.84
3.6	14.09	3.2	10.77	3	3.088	3.6	3.33	2.6	9.008	2.4	2.38	2.4	3.775	2	1.68
3.8	19.35	3.4	19.6	3.2	6.612	3.8	4.33	2.8	10.16	2.6	4.29	2.5	10.02	2.1	6.72
4	23.66	3.6	27.23	3.4	10.92	4	5.33	3	12.06						

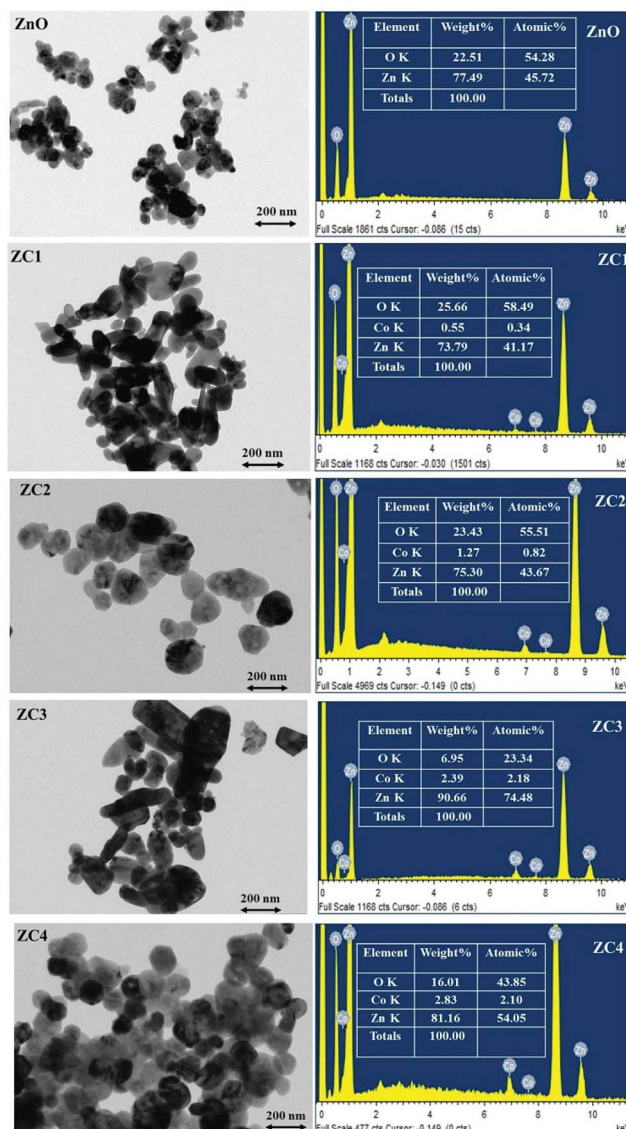


Fig. 3 XRD pattern of  $\text{Zn}_{1-x}\text{CoxO}$  nanopowders.Fig. 4 W-H plots and crystallite size of  $\text{Zn}_{1-x}\text{CoxO}$  nanopowders at different doping concentrations.<sup>25</sup>

size ( $D$ ) of nanoparticles were estimated using Williamson and Hall (W-H) plot (Fig. 4) from the Cauchy-Lorentzian relation.<sup>25</sup>

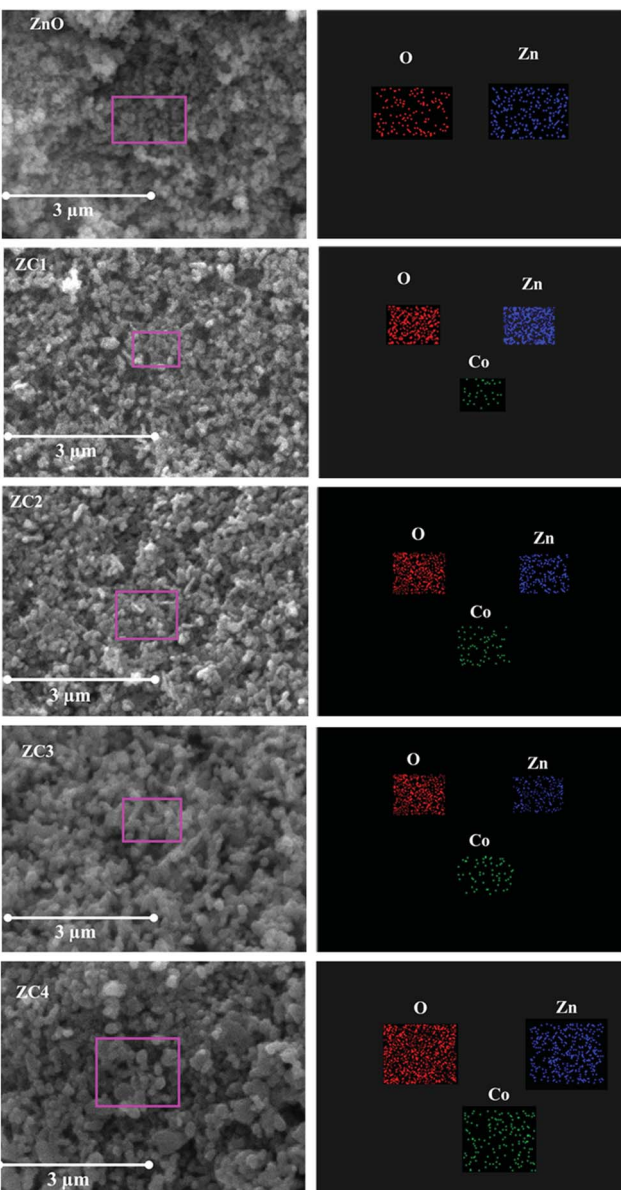
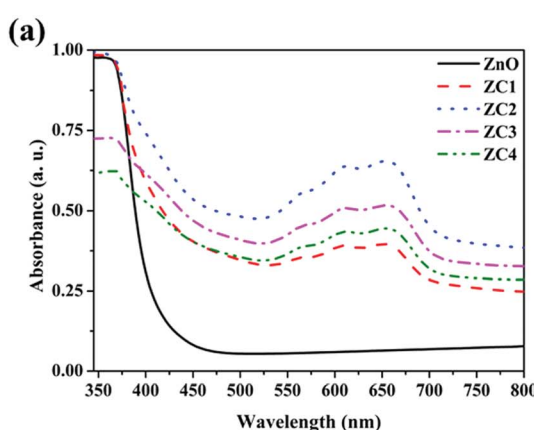
$$\beta \cos \theta = \frac{C\lambda}{D} + 4\epsilon \sin \theta \quad (1)$$

where,  $C$  is the shape factor,  $\theta$  is the diffraction angle and  $\lambda$  is the X-ray wavelength. The change in crystallite size with alloy composition is shown in Fig. 4. An increase in crystallite size was observed with increase in concentration of Co (Fig. 5), which is similar to the previously reported studies.<sup>26</sup> However as

Fig. 5 TEM and EDS data of  $\text{Zn}_{1-x}\text{CoxO}$  nanopowders.

the doping concentration increased up to 4 at% a reduction in size was seen, which may be due to the hindrance in grain growth or grain splitting effect with more Co concentration.<sup>27</sup>

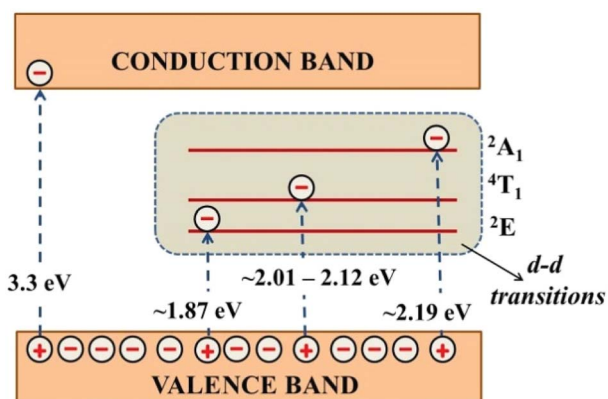
The morphology of the nanoparticles obtained using TEM imaging and the elemental composition determined using EDS analysis is shown in Fig. 5. Homogeneously distributed disc shaped nanoparticles with an average diameter in the range of 40–50 nm was observed from TEM analysis. All the compositions, the morphology of the system is found to be same and also the size distributions between the nanodiscs of different compositions are found to be in narrow range which will not remarkably affect the system efficiency. EDS analysis confirmed the presence of Zn, Co and O in the synthesized nanopowders. The atomic percentage obtained from EDS is shown in the inset of Fig. 5. Elemental mapping was performed to view the relative elemental distribution in nanoparticles and is revealed in Fig. 6. It shows that the elements Zn, O and CO are homogeneously distributed and also clearly depicts the increase in

Fig. 6 Elemental mapping of  $Zn_{1-x}Co_xO$  nanopowders.Fig. 7 (a) Absorbance and (b) reflectance spectra of  $Zn_{1-x}Co_xO$  nanopowders.

concentration of Co atoms in the nanoparticle upon increasing the doping concentration.

Fig. 7a and b shows the optical absorbance and reflectance spectra of  $Zn_{1-x}Co_xO$  nanoparticles recorded in DRS mode, respectively. With Co doping, the three characteristic absorption peaks corresponds to the d-d transition of  $Co^{2+}$  ions in tetrahedral co-ordination has been observed (563 nm, 610 nm and 657 nm) in the visible region.<sup>28</sup> This confirms that most of the  $Co^{2+}$  occupies the  $Zn^{2+}$  sites in  $ZnO$  lattice, rather than precipitating as cobalt oxide ( $CoO$ ) or Co metal.<sup>29</sup> The series of absorption is due to the crystal field transitions from  $^2A_1$ ,  $^4T_1$  and  $^2E$  multiplets.<sup>20</sup> Fig. 8 shows the schematic of absorption levels of  $Co^{2+}$  ions in  $ZnO$  lattice. The intensity of these peaks and UV absorption peak is found to be increased with Co doping up to 2% and then decreases due to the increased Co content.<sup>24</sup> The decreased absorption in ZC3 might also have resulted from the increased agglomeration as seen from the TEM images which reduces the surface area for absorption.<sup>30</sup> For 4% doping, the decreased crystallinity indicated by the reduced XRD peak intensity of ZC4 may also be a reason behind the decrease in absorbance.<sup>24</sup>

From the DRS data the bandgap of  $Zn_{1-x}Co_xO$  nanopowders was estimated using Kubelka Monk relation,<sup>31</sup>

Fig. 8 Schematic of  $Co^{2+}$  absorption levels in  $ZnO$  lattice.

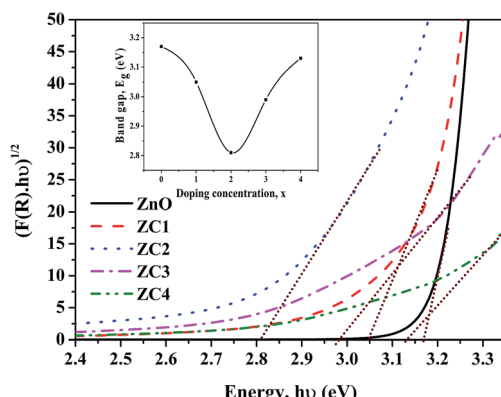


Fig. 9 Kubelka monk plot for  $\text{Zn}_{1-x}\text{CoxO}$  nanopowders (inset: bandgap variation of  $\text{Zn}_{1-x}\text{CoxO}$  nanopowders with doping concentration).

$$F(R) = \frac{1 - R^2}{2R} \quad (2)$$

where,  $F(R)$  is the Kubelka Munk function and  $R$  is the reflectance. The inset of Kubelka Monk plot (Fig. 9) shows the bandgap variation with doping concentration. It can be seen that the bandgap of  $\text{ZnO}$  has decreased with the incorporation of  $\text{Co}^{2+}$  ions, which can be attributed to the decrease of spin-up band.<sup>32</sup> Further, the red shift is seen to be less at higher concentration, which can be due to the influence of Burstein–Moss effect.<sup>27</sup>

From the DRS data the optical conductivity ( $\sigma$ ) of the  $\text{Zn}_{1-x}\text{CoxO}$  nanopowders at each source wavelengths were estimated using the relations.<sup>33</sup>

$$R(\sigma) = \omega I(\varepsilon) \varepsilon_0 \quad (3)$$

$$I(\sigma) = \omega R(\varepsilon) \varepsilon_0 \quad (4)$$

where,  $\omega = (2c/\lambda)$  is the angular frequency,  $c$  is the velocity of light,  $\varepsilon$  is the permittivity and  $\varepsilon_0$  is the permittivity of free space. Fig. 10 shows that the improvement in the optical conductivity

of  $\text{ZnO}$ , at smaller concentrations of Co doping which is in line with the previous reports.<sup>24,34</sup> Johnson *et al.* reported that this increase in photoconductivity with Co incorporation can be further enhanced at higher temperatures by a thermally assisted ionization process. Since our work focus on room temperature photodetection, variable temperature studies have not been performed.<sup>35</sup>

Further, to confirm the presence of elements and to examine its chemical states in the obtained nanopowders, XPS study has been carried out. C 1s hydrocarbon photoelectron peak at 284.6 eV is used as reference for analysis. Fig. 11a represents the survey spectrum of ZC2, which shows the existence of Co ions in  $\text{ZnO}$  with obtained peaks around 779.32 eV and 795.83 eV corresponding to the  $2p_{3/2}$  and  $2p_{1/2}$  electronic states.<sup>36</sup>

The high resolution spectra of Zn 2p, O 1s and Co 2p are given in Fig. 11b, c and d, respectively. Due to strong spin orbit coupling, the Zn 2p peaks have been split into two at 1020.35 eV and 1043.43 eV which can be assigned to the  $2p_{3/2}$  and  $2p_{1/2}$  binding states.<sup>37</sup> Moreover, the energy difference of  $\sim 23$  eV

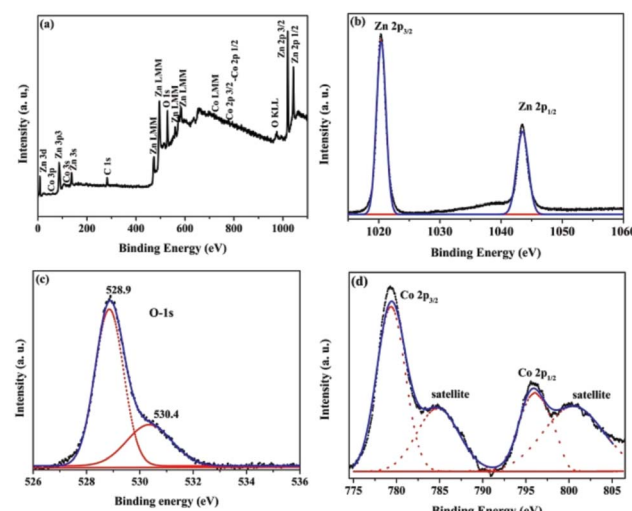


Fig. 11 (a) XPS survey spectrum of  $\text{Zn}_{0.98}\text{Co}_{0.02}\text{O}$  nanoparticles, (b), (c) and (d) high resolution spectra of Zn, O and Co, respectively.

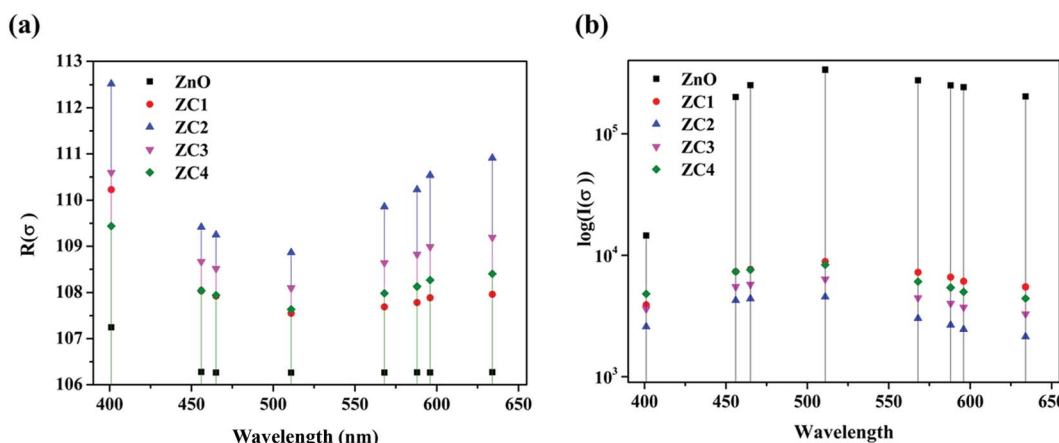


Fig. 10 (a) Real and (b) log or imaginary part of conductivity of  $\text{Zn}_{1-x}\text{CoxO}$  nanopowders.

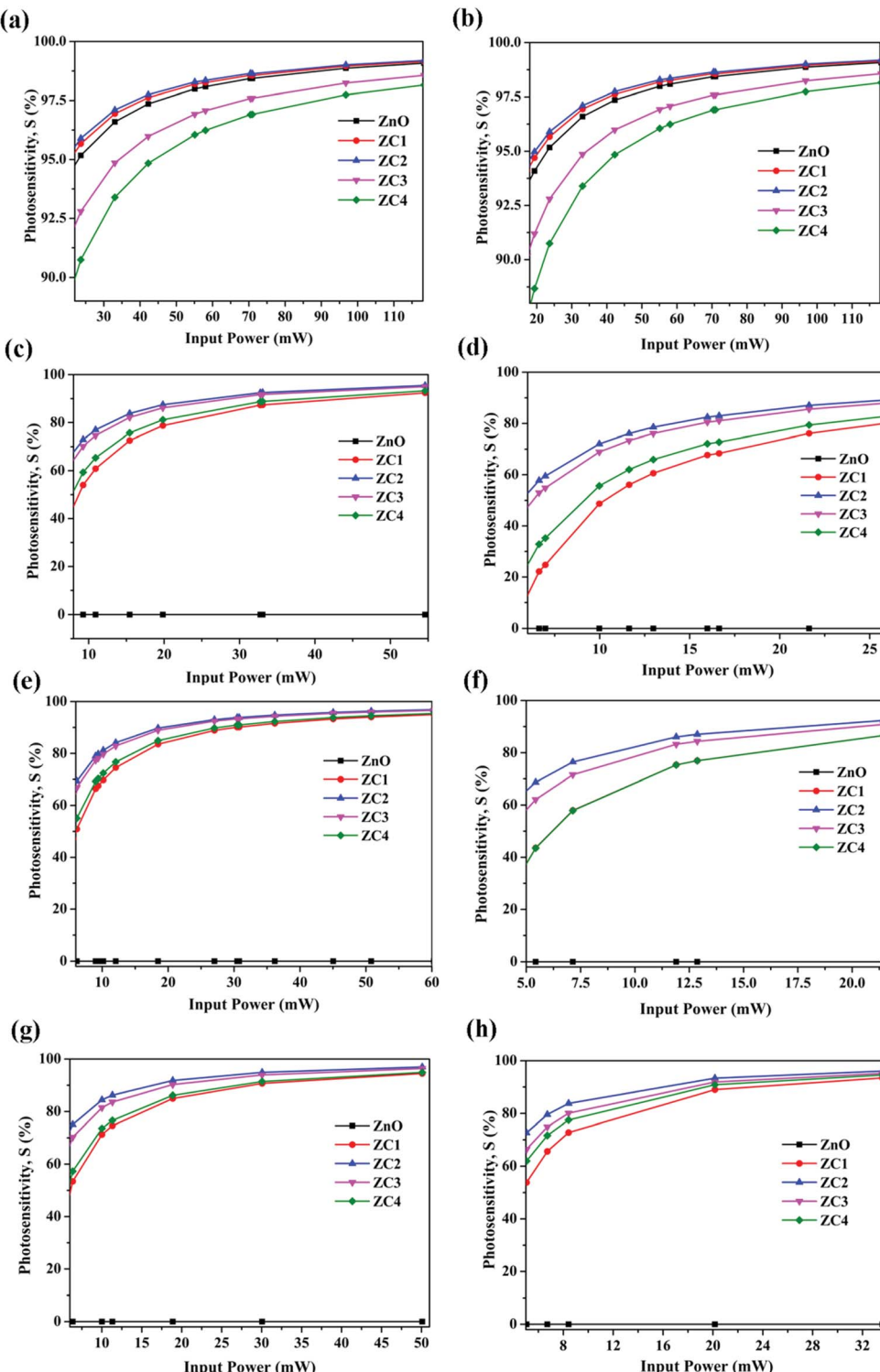


Fig. 12 Photosensitivity of fabricated PDs towards LED sources (a) 401 nm (b) 456 nm (c) 465 nm (d) 511 nm (e) 570 nm (f) 588 nm (g) 598 nm and (h) 634 nm towards varying input power.

between two peaks is in well agreement with the standard value of ZnO and it strongly indicates the +2 oxidation state of Zn.<sup>38</sup> The high resolution O 1s spectra can be resolved into two components at 528.9 eV and 530.4 eV which corresponds to the O<sup>2-</sup> ions in the Zn<sub>0.98</sub>Co<sub>0.02</sub>O lattice (Zn–O, Co–O bonds) and the adsorbed oxygen on the Zn<sub>0.98</sub>Co<sub>0.02</sub>O nanopowder surface, respectively.<sup>39,40</sup> In the high resolution spectra of Co, the energy difference of ~16 eV between the energy states confirms the incorporation of cobalt ions into ZnO lattice at +2 oxidation state.<sup>41</sup> In addition to the two major peaks at 779.08 eV and 795.7 eV due to spin orbit splitting of cobalt, two satellite peaks located at ~785 eV and ~800 eV were appeared. These

characteristic peaks also known as shake-up resonance transitions resulted from the transition of valence electrons and core holes.<sup>36,40</sup> XPS and XRD investigations concurrently confirms that  $\text{Co}^{2+}$  ions have been incorporated into ZnO lattice by substituting  $\text{Zn}^{2+}$  ions with no additional phase or impurities.

### 3.2. Photoreponse studies

The photodetection studies of the fabricated PDs were performed under dark, NUV and different visible wavelength light sources. The LEDs were kept at a distance of 4 cm from the PDs biased at 5 V and the photocurrent was measured at different input powers.

The photosensitivity ( $S$ ) was calculated from the obtained dark and light environment resistance values  $R_d$  and  $R_l$ , respectively for different source power as,

$$S (\%) = \left( \frac{R_d - R_l}{R_d} \right) \times 100\% \quad (5)$$

The photoresponse of PDs towards different wavelength was seen to be consistent with the obtained DRS optical response (Fig. 12). The parameters responsivity ( $R$ ) and quantum efficiency ( $\eta$ ) of the PDs at different wavelengths were calculated using the relations,<sup>42</sup>

$$R = \frac{I_l - I_d}{P_{in}} \quad (6)$$

$$\eta = \frac{Rhc}{e\lambda} \quad (7)$$

where,  $I_d$  and  $I_l$  are the photocurrents under dark and light conditions, respectively.  $P_{in}$  is the power input to PD,  $h$  is the Plank's constant,  $c$  is the velocity of light,  $e$  is the electron charge and  $\lambda$  is the source wavelength. The  $R$  and  $\eta$  values of PDs at different wavelengths are shown in Fig. 13a and b. In the NUV regime, ZC1 and ZC2 PDs exhibited enhanced photoresponse and increased  $\eta$  compared to ZnO PD, which is due to the

improvement in photoconductivity of ZnO (as seen in Fig. 10) by doping with smaller concentration of transition metal. Also, due to the shift in absorption edge and presence of absorption bands arose from ligand field split states, appreciable visible light absorption is obtained with Co doping. As expected from the optical spectrum, the visible absorption is increased up until 2% doping of Co and decreased with further increase in concentration. In the visible regime, all the Co doped ZnO PDs showed good response, whereas towards higher wavelengths ( $>565$  nm) the PDs exhibit better response due to the d-d transition of  $\text{Co}^{2+}$  ions. Thus doping with Co at lower concentration can significantly enhance the photoresponsivity of ZnO PDs in NUV and visible regime.

Literature reports show the fabrication of various photodetectors based on ZnO nanostructures with different architectures and synthesis methods. Due to the wide bandgap, pure ZnO itself acts as a good UV detector. Dopants like magnesium,<sup>42-45</sup> iron,<sup>46</sup> vanadium,<sup>47</sup> gallium,<sup>48</sup> lanthanum,<sup>49</sup> manganese,<sup>50</sup> antimony,<sup>51</sup> titanium,<sup>15</sup> etc., in ZnO have been reported for the improvement of ZnO response in the UV region. When it comes to visible detection, the reports on successful fabrication of visible detectors based on ZnO are very scarce. Our first attempt for the fabrication of ZnO based visible detector was with cadmium (Cd) doping, which red shifted the band gap and extended the detection up to blue region (2.66 eV). But further shifting towards visible region was still not feasible.<sup>19</sup> In the present work, Co doping improves detection in multiple visible bands simultaneously with UV, which is a remarkable achievement for the various applications of visible detectors as discussed in the introduction. Merging with other functionalities or technologies like plasmonic enhancement, self-powering, portable PDs which stands on flexible electronics the performance of these detectors can be still improved.<sup>49,50,52-58</sup>

Fig. 14 shows the efficiency of fabricated PDs at different wavelengths. Compared to pure ZnO, an increase of  $\sim 3\%$  and 4% was obtained with ZC1 and ZC2 PDs respectively in the NUV regime. Remarkable visible light response was observed with all

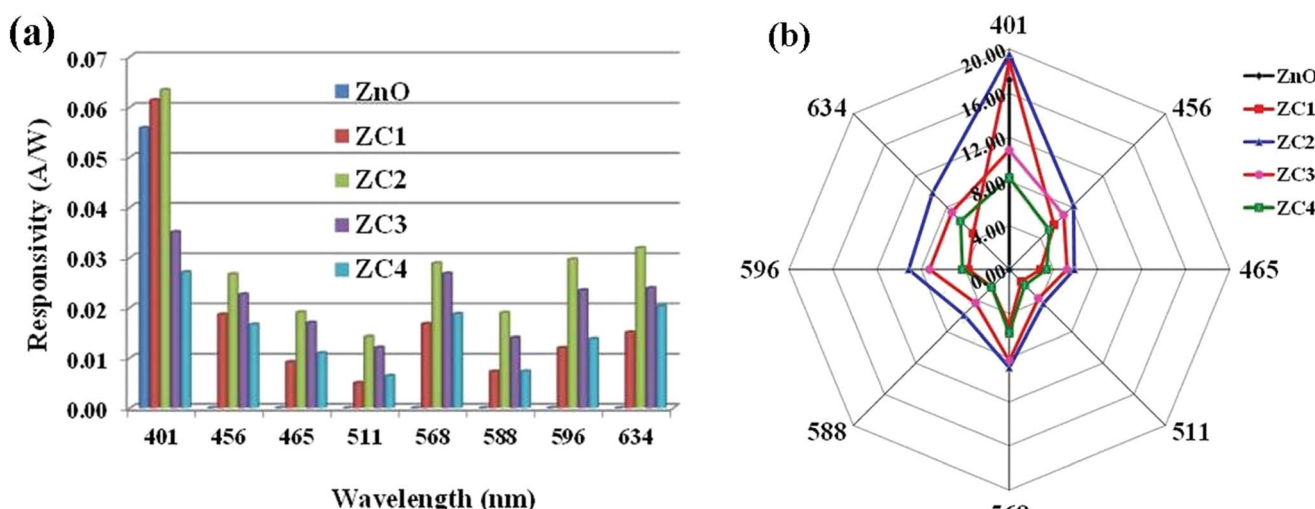


Fig. 13 (a) Responsivity and (b) quantum efficiency of the fabricated photodetectors.



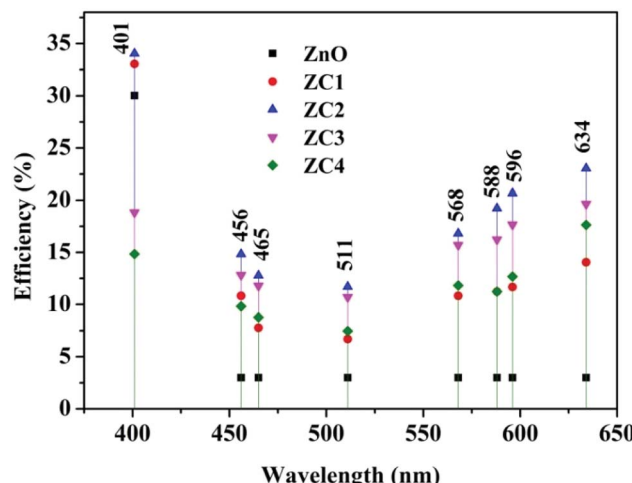


Fig. 14 Efficiency of fabricated photodetectors.

PDs, especially at higher wavelengths. Among all, ZC2 PD exhibited higher photoresponse in NUV as well visible region, for which an efficiency of 23% was achieved at 634 nm. These results give a strong foundation for the fabrication of Co doped ZnO NUV-Vis PDs for various applications. Though silicon (1.1 eV) and germanium (0.67 eV) based light detectors are commercially available, the low band gaps lead to undesirable near-IR light response which has to be eliminated and that again complex the architecture and increases the expenditure.<sup>59</sup> This study proposes a panacea for the design of efficient visible light detection at multiple energy bands.

## 4. Conclusions

$Zn_{1-x}Co_xO$  ( $x = 0, 1, 2, 3 \& 4$ ) nanoparticles having hexagonal wurtzite structure were synthesized by co-precipitation method. Upon Co doping in addition to the NUV absorption, broad visible absorptions around  $\sim 571$  nm, 618 nm and 682 nm has also been observed due to d-d transition of  $Co^{2+}$  ions. At the Co doping concentration of 1 and 2%, the near UV detection efficiency of PDs was improved by 3–4% and  $Zn_{0.98}Co_{0.02}O$  gave a maximum responsivity value of about  $63 \text{ mA W}^{-1}$ . The  $Zn_{1-x}Co_xO$  PDs showed good response to visible lights among which  $x = 2$  exhibited maximum efficiency of 23% at 634 nm. Thus, the advantage of ligand field splitting states of Co doped ZnO in the visible region was utilized for the fabrication of ZnO based NUV-Vis PDs. The investigation from this work put forwards that the efficient visible photodetectors with enhanced photoabsorption can be fabricated with Co doped ZnO nanoparticles. Combining with other functionalities or technologies like self-powered PDs, portable PDs with flexible electronics etc., fabrication of still improved visible light PDs can be achieved.

## Conflicts of interest

There are no conflicts to declare.

## Acknowledgements

The authors would like to acknowledge the Department of Science and technology (DST), New Delhi, India for providing the financial support through FIST (Fund for Improvement of S&T Infrastructure in Higher Educational Institutions) project [SR/FST/ETI-015/2011].

## References

- 1 N. Bi, L. Zhang, Q. Zheng, F. Zhuge, J. Li, X. P. Gao and J. Du, *J. Mater. Sci. Technol.*, 2017, DOI: 10.1016/j.jmst.2017.03.024.
- 2 M. Cao, F. Wang, J. Zhu, X. Zhang, Y. Qin and L. Wang, *Mater. Lett.*, 2017, **192**, 1.
- 3 M. Kahouli, A. Barhoumi, A. Bouzid, A. Al-Hajry and S. Guermazi, *Superlattices Microstruct.*, 2015, **85**, 7.
- 4 A. Bedia, F. Z. Bedia, M. Aillerie, N. Maloufi and B. Benyoucef, *Energy Procedia*, 2015, **74**, 529.
- 5 G. H. He, H. Zhou, H. Shen, Y. J. Lu, H. Q. Wang, J. C. Zheng, B. H. Li, C. X. Shan and D. Z. Shen, *Appl. Surf. Sci.*, 2017, **412**, 554.
- 6 A. Bedia, F. Z. Bedia, B. Benyoucef and S. Hamzaoui, Electrical characteristics of ultraviolet photodetector based on ZnO nanostructures, *Phys. Procedia*, 2014, **55**, 53.
- 7 Z. Zhang, Q. Liao, Y. Yu, X. Wang and Y. Zhang, *Nano Energy*, 2014, **9**, 237.
- 8 H. Chen, K. Liu, L. Hu, A. A. Al-Ghamdi and X. Fang, *Mater. Today*, 2015, **18**, 493.
- 9 T. Makino, Y. Segawa, M. Kawasaki, A. Ohtomo, R. Shiroki, K. Tamura, T. Yasuda and H. Koinuma, *Appl. Phys. Lett.*, 2001, **78**, 1237.
- 10 Y. Wang, J. Chen, S. Yu, E. J. Alcocer, M. Shahid, Z. Wang and W. Pan, *Sci. Rep.*, 2016, **6**, 2.
- 11 N. Nithya and S. R. Radhakrishnan, *International Journal of Engineering Research and Technology*, 2013, **2**, 1649.
- 12 J. S. Shiau, S. Brahma, C. P. Liu and J. L. Huang, *Thin Solid Films*, 2016, **620**, 170.
- 13 J. D. Hwang, S. Y. Wang and S. B. Hwang, *J. Alloys Compd.*, 2016, **656**, 618.
- 14 P. S. Shewale and Y. S. Yu, *Ceram. Int.*, 2016, **42**, 7125.
- 15 P. S. Shewale and Y. S. Yu, *J. Alloys Compd.*, 2016, **654**, 79.
- 16 L. U. Khan, *Digital Communications and Networks*, 2017, **3**, 78.
- 17 S. Gowrishankar, L. Balakrishnan and N. Gopalakrishnan, *Ceram. Int.*, 2014, **40**, 2135.
- 18 N. Kumar and A. Srivastava, *J. Alloys Compd.*, 2017, **706**, 438.
- 19 A. A. Jacob, L. Balakrishnan, S. R. Meher, K. Shambavi and Z. C. Alex, *J. Alloys Compd.*, 2017, **695**, 3753.
- 20 P. Koidl, *Phys. Rev. A*, 1977, **15**, 2493.
- 21 V. Y. Ivanov, A. J. Zakrzewski, B. S. Witkowski and M. Godlewski, *Opt. Mater.*, 2016, **59**, 15.
- 22 H. Yang and S. Nie, *Mater. Chem. Phys.*, 2009, **114**, 279.
- 23 W. Li, G. Wang, C. Chen, J. Liao and Z. Li, *Nanomaterials*, 2017, **7**, 20.
- 24 C. A. Johnson, A. Cohn, T. Kaspar, S. A. Chambers, G. M. Salley and D. R. Gamelin, *Phys. Rev. B: Condens. Matter Mater. Phys.*, 2011, **84**, 125203.



25 A. A. Akl and A. S. Hassanien, *Int. J. Adv. Res.*, 2014, **2**, 1.

26 M. G. Nair, M. Nirmala, K. Rekha and A. Anukaliani, *Mater. Lett.*, 2011, **65**, 1797.

27 S. A. Ansari, A. Nisar, B. Fatma, W. Khan and A. H. Naqvi, *Mater. Sci. Eng., B*, 2012, **177**, 428.

28 R. He, B. Tang, C. Ton-That, M. Phillips and T. Tsuzuki, *J. Nanopart. Res.*, 2013, **15**, 2030.

29 M. Shatnawi, A. M. Alsmadi, I. Bsoul, B. Salameh, G. A. Alna'washi, F. Al-Dweri and F. El Akkad, *J. Alloys Compd.*, 2016, **655**, 244.

30 S. Sakthivel, B. Neppolian, M. V. Shankar, B. Arabindoo, M. Palanichamy and V. Murugesan, *Sol. Energy Mater. Sol. Cells*, 2003, **77**, 65.

31 F. Yakuphanoglu, *J. Alloys Compd.*, 2010, **507**, 184.

32 H. Yang and S. Nie, *Mater. Chem. Phys.*, 2009, **114**, 279.

33 J. N. Hodgson, *Optical absorption and dispersion in solids*, Springer Science & Business Media, 2012.

34 W. K. Liu, G. M. Salley and D. R. Gamelin, *J. Phys. Chem. B*, 2005, **109**, 14486.

35 C. A. Johnson, T. C. Kaspar, S. A. Chambers, G. M. Salley and D. R. Gamelin, *Phys. Rev. B: Condens. Matter Mater. Phys.*, 2010, **81**, 125206.

36 Z. K. Heiba and L. Arda, *J. Mol. Struct.*, 2012, **1022**, 167.

37 N. L. Tarwal, K. V. Gurav, T. P. Kumar, Y. K. Jeong, H. S. Shim, I. Y. Kim, J. H. Kim, J. H. Jang and P. S. Patil, *J. Anal. Appl. Pyrolysis*, 2014, **106**, 26.

38 C. D. Wagner, W. M. Riggs, L. E. Davis, J. F. Moulder and G. E. Mulenberg, *Handbook of X-ray Photoelectron Spectroscopy*, Perkin-Elmer Co., 1979, p. 82.

39 M. Chen, X. Wang, Y. H. Yu, Z. L. Pei, X. D. Bai, C. Sun, R. F. Huang and L. S. Wen, *Appl. Surf. Sci.*, 2000, **158**, 134.

40 Y. Zhu, G. Xu, T. Guo, H. Hou and S. Tan, *J. Alloys Compd.*, 2017, **720**, 105.

41 S. Deka and P. A. Joy, *Solid State Commun.*, 2005, **134**, 665.

42 P. S. Shewale and Y. S. Yu, *J. Alloys Compd.*, 2016, **654**, 79.

43 Y. H. Liu, S. J. Young, L. W. Ji, T. H. Meen, C. H. Hsiao, C. S. Huang and S. J. Chang, *IEEE Trans. Electron Devices*, 2014, **61**, 1541.

44 Y. H. Liu, S. J. Young, L. W. Ji and S. J. Chang, *IEEE J. Sel. Top. Quantum Electron.*, 2015, **21**, 223.

45 Y. Hou, Z. Mei and X. Du, *J. Phys. D: Appl. Phys.*, 2014, **47**, 283001.

46 A. Khayatian, V. Asgari, A. Ramazani, S. F. Akhtarianfar, M. A. Kashi and S. Safa, *Mater. Res. Bull.*, 2017, **94**, 77.

47 B. B. Deka and A. Misra, *ACS Appl. Mater. Interfaces*, 2016, **8**, 18182.

48 S. S. Shinde and K. Y. Rajpure, *Appl. Surf. Sci.*, 2011, **257**, 9595.

49 C. L. Hsu, H. H. Li and T. J. Hsueh, *ACS Appl. Mater. Interfaces*, 2013, **5**, 11142.

50 C. O. Chey, X. Liu, H. Alnoor, O. Nur and M. Willander, *Phys. Status Solidi RRL*, 2015, **9**, 87.

51 S. V. Mohite and K. Y. Rajpure, *Opt. Mater.*, 2014, **36**, 833.

52 R. Yang, A. Sazonov and V. Karanassios, in *Sensors IEEE*, 2016, p. 3.

53 R. Ishimatsu, A. Naruse, R. Liu, K. Nakano, M. Yahiro, C. Adachi and T. Imato, *Talanta*, 2013, **117**, 139.

54 O. Game, U. Singh, T. Kumari, A. Banpurkar and S. Ogale, *Nanoscale*, 2014, **6**, 503.

55 Y. Guo, Y. Li, Q. Zhang and H. Wang, *J. Mater. Chem. C*, 2017, **5**, 1436.

56 G. Gu, N. Mojaverian, J. Vaillancourt and X. Lu, *J. Phys. D: Appl. Phys.*, 2014, **47**, 435106.

57 H. Wang, J. W. Lim, F. M. Mota, Y. J. Jang, M. Yoon, H. Kim, W. Hu, Y. Y. Noh and D. H. Kim, *J. Mater. Chem. C*, 2017, **5**, 399.

58 S. B. Wang, R. S. Chen, S. J. Chang, H. C. Han, M. S. Hu, K. H. Chen and L. C. Chen, *Nanoscale*, 2014, **6**, 1264.

59 Q. Lin, A. Armin, D. M. Lyons, P. L. Burn and P. Meredith, *Adv. Mater.*, 2015, **27**, 2060.

